Effect of grain boundary sliding on the toughness of ultrafine grain structure steel: A molecular dynamics simulation study

Xie Hong-Xian(谢红献)[a)†], Liu Bo(刘 波)[a)], Yin Fu-Xing(殷福星)[b)], and Yu Tao(于 涛)[c)]

[a)] School of Mechanical Engineering, Hebei University of Technology, Tianjin 300132, China
[b)] Materials Research Institute for Energy Equipments, China First Heavy Industries, Qiqihar 161042, China
[c)] Central Iron and Steel Research Institute, Beijing 100081, China

(Received 10 June 2012; revised manuscript received 26 June 2012)

Molecular dynamics simulations are carried out to investigate the mechanisms of low-temperature impact toughness of the ultrafine grain structure steel. The simulation results suggest that the sliding of the {001}/{110} type and {110}/{111} type grain boundary can improve the impact toughness. Then, the mechanism of grain boundary sliding is studied and it is found that the motion of dislocations along the grain boundary is the underlying cause of the grain boundary sliding. Finally, the sliding of the grain boundary is analyzed from the standpoint of the energy. We conclude that the measures which can increase the quantity of the {001}/{110} type and {110}/{111} type grain boundary and elongate the free gliding distance of dislocations along these grain boundaries will improve the low-temperature impact toughness of the ultrafine grain structure steel.

Keywords: molecular dynamics simulations, grain boundary, crack, ultrafine grain structure steel

PACS: 02.70.Ns, 83.60.Uv, 61.72.Ff **DOI:** 10.1088/1674-1056/22/1/010204

1. Introduction

Steel is the king of structural materials. Strong and tough steels are always in demand to reduce weight, improve safety in transportation and performance in heavy machinery, and enhance architectural flexibility in construction.[1] However, steel usually loses most of its ductility and fractures in a brittle mode when the temperature falls below the ductile-to-brittle transition temperature (DBTT). That is to say, the steel will fracture in a moment, often leading to serious accidents. Thus, it is very important to develop some methods to lower the DBTT.

The refinement of crystalline grain size is considered to be a method of lowering the DBTT for high-strength metals.[2–6] However, when the grain size is close to 1 μm or less, the toughness and tensile ductility at room temperature will become low.[6–9] The delamination is another method of lowering the DBTT for high-strength metals. However, the delamination toughening typically sacrifices toughness in the ductile fracture region for a reduction of DBTT.[7,10,11]

Recently, by combining grain refinement and delamination, Kimura *et al.* developed an ultrahigh-strength low-alloy bcc steel bar with excellent toughness at lower temperatures.[12–15] The microstructures in the central parts of the cross sections of the bar were observed by using the electron backscattered diffraction (EBSD).[14] They also found that it has ultrafine grain structures that consist of elongated grains with strong ⟨110⟩ (rolling direction, RD), ⟨001⟩, ⟨101⟩, and ⟨111⟩ (striking direction, SD) fiber deformation textures (see Fig. 1 in Ref. [14]). After the Charpy V-notch impact test, the sample was observed and found to exhibit delamination, which signifies that cracks branched were parallel to the longitudinal direction of the impact test bars, and therefore the crack propagations in the SD were substantially blunted (see Fig. 1 in Ref. [14]). Delamination of the bar has been explained as follows: bcc iron mainly cleaves on {100} planes, and the {100}⟨110⟩ fiber deformation textures provide lots of cleavage {100} orientations parallel to the RD of the impact bar. This causes delaminating cracks perpendicular to the SD.[13]

Experimental studies have shown that the initial crack, which propagates along the SD direction, will turn its way from the SD direction into the RD direction, leading to a delaminating crack. However, as far as we know, the reason for the turning of the crack's propagation direction has not been expounded in the literature. Furthermore, the impact bar is composed of {100}⟨110⟩, {110}⟨110⟩, and {111}⟨110⟩ fiber deformation textures, and thus there are abundant grain boundaries between two elongated grains with different texture components. The grain boundaries may cleave more easily than {100} planes, and offer delaminating places to the steel bar. To the best of our knowledge, however, the effect of grain boundaries on the toughness of the steel bar has not been fully understood yet.

In the present work, the molecular dynamics (MD) method, as a powerful tool to study the nature of materials,[16–19] is used to investigate the effect of grain boundaries on the low-temperature toughness of the ultrafine grain structure steel. Moreover, the effect of grain boundary sliding

†Corresponding author. E-mail: hongxianxie@163.com

© 2013 Chinese Physical Society and IOP Publishing Ltd

on the toughness of the steel bar will be carefully explored. This paper is organized as follows: in Section 2, we briefly describe the conditions of molecular dynamics simulation; in Section 3 we present structure evolution of the six crack models; Section 4 is devoted to the mechanisms of grain boundary gliding. Finally, conclusions are presented in Section 5.

2. Conditions of computer simulations

The molecular dynamics simulations were performed by using a parallel MD code, LAMMPS, developed by Plimpton and co-workers.[20,21] In the simulation, many-body interatomic potential was used to calculate Fe–Fe interatomic forces based on the embedded atom method (EAM) developed by Mendelev *et al.*[22] This potential was developed by fitting to the first-principle forces obtained in a model liquid configuration and also to other experimentally obtained material properties. Recently, a number of results obtained by using four Fe potentials were compared between themselves and with available experimental (or first-principle DFT) data.[23] It was found that the Mendelev potential provides a good qualitative agreement with a large body of experimental and *ab initio* calculation data for iron, including the elastic modulus, the energy of point defects, the bcc–fcc transition energy, the lattice parameter of α-Fe for several temperatures, the density of structure factor of the liquid phase, and the melting temperature.

From the observation of EBSD, we know that the steel bar consists of three kinds of elongated grains. All the elongated directions of grains are along the $\langle 110\rangle$ crystal orientation (parallel to the RD), and the crystal orientations of grains that are parallel to the SD are $\langle 001\rangle$, $\langle 101\rangle$, and $\langle 111\rangle$, respectively. Hence, there can exist three kinds of grain boundary which are parallel to the RD. Based on the above analysis, six models are constructed to study the effect of grain boundary on the crack propagation (see Fig. 1 and Table 1). All of the six models are oriented with $[1\bar{1}0]$ along the y direction (parallel to the RD). In order to use the periodic boundary condition along the z direction, the size of the part I along the z-axis direction and that of the part II along the z-axis direction should meet the following relation:

$$ma_{[x_1y_1z_1]} = na_{[x_2y_2z_2]}, \tag{1}$$

where m and n are integer, $a_{[x_1y_1z_1]}$ and $a_{[x_2y_2z_2]}$ are the lengths of the conventional unit cell along the $[x_1y_1z_1]$ and $[x_2y_2z_2]$ directions, respectively. The $ma_{[x_1y_1z_1]}$ is the size of the part I in the z direction and $na_{[x_2y_2z_2]}$ is the size of the part II in the z direction. In the present work, the difference of the size between the two parts in the z direction is no more than 2%, and probably has no effect on the simulation results. The initial uncracked models are relaxed via conjugate gradient energy minimization. During the relaxation, only the box dimension along the direction normal to the GB (along the x direction) is allowed to relax in order to alleviate any GB pressure. Then the pre-existing crack of model-I type with length $l_0 = 15$ nm is introduced according to the continuum theory by shifting the atoms from their positions in a perfect crystal to positions specified by the anisotropic elasticity continuum mechanics equations,[24] for the desired stress intensity K. After the initial configurations of the crack are obtained, the atoms of the cracked models are fully relaxed via conjugate gradient energy minimization with the fixed-displacement boundary condition in the y direction and the periodic boundary conditions in the z direction.

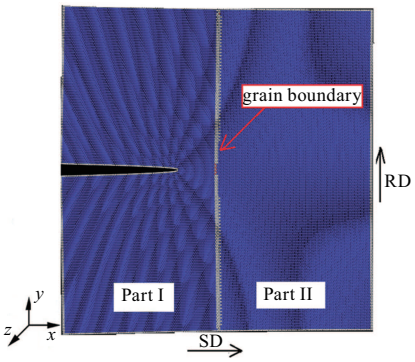


Fig. 1. (color online) Schematic illustration of the original crack.

To entice the crack to evolve, four top and four bottom layers of atoms in the y direction are loaded by external stress $\sigma_{\text{ext}} = 3.3$ GPa. Periodic boundary conditions are imposed in the crack front (z direction), while free boundary

Table 1. Atomic configurations of the initial six models. The grain boundary is specified by the two sides of crystal orientations that are parallel to the x direction.

Model	Part I $x \times y \times z$	Part II $x \times y \times z$	Number of total atoms	Type of grain boundary
A	$70[001] \times 100[1\bar{1}0] \times 5[110]$	$50[110] \times 100[1\bar{1}0] \times 7[001]$	280000	–
B	$50[110] \times 100[1\bar{1}0] \times 7[001]$	$70[001] \times 100[1\bar{1}0] \times 5[110]$	280000	{001}/{110}
C	$50[110] \times 100[1\bar{1}0] \times 5[001]$	$40[111] \times 100[1\bar{1}0] \times 2[11\bar{2}]$	196000	–
D	$40[111] \times 100[1\bar{1}0] \times 2[11\bar{2}]$	$50[110] \times 100[1\bar{1}0] \times 5[001]$	196000	{110}/{111}
E	$40[111] \times 100[1\bar{1}0] \times 4[11\bar{2}]$	$70[001] \times 100[1\bar{1}0] \times 7[110]$	388000	–
F	$70[001] \times 100[1\bar{1}0] \times 7[110]$	$40[111] \times 100[1\bar{1}0] \times 4[11\bar{2}]$	388000	{001}/{111}

conditions are applied in the x axis (the direction of crack propagation). At the beginning of simulations and before applying the external forces, a Gaussian distribution of the velocities of all atoms is generated by using a random number generator at a specific temperature (10 K). The simulations are performed in a constant NVE ensemble. Atomic accelerations, velocities, and positions are updated at each time step using the Velocity–Verlet algorithm. The total simulation time is 50 ps with a time step of 0.005 ps.

The visualization of the simulation results was conducted by using the common neighbor analysis (CNA) method[25] and implemented in the OVITO program.[26] The analysis and classification of each atom according to its environment (hcp, fcc, bcc, bcc twins, or undefined) allow us to identify various deformation mechanisms occurring in the crack-tip region. In particular, a great advantage of this analysis is that it enables the easy visualization of dislocation emission, twin formation, as well as phase transformations.

3. Results and discussion

3.1. Effect of {001}/{110} grain boundary on the propagation of the crack

3.1.1. Model A

Figure 2 gives the details of the atomistic process of the crack propagation through the {001}/{110} grain boundary from the {001} part to the {110} part (the parts on both sides of the grain boundary are specified by the crystal orientations that are parallel to the x direction). The initial crack type is $\{1\bar{1}0\}\langle 110\rangle$ (specified by the crack plane and the crack front). From this figure, it can be observed that before the crack reaches the grain boundary (see Fig. 2(a)), there is a plastic region in front of the crack tip, and the atoms in this region are disordered rather than keeping bcc structure. However, the crack propagates forward, driven by something like a brittle manner because no dislocation emits from the crack tip. When the plastic region reaches the grain boundary (see Fig. 2(b)), the grain boundary begins to glide along the y direction. As a result, the crack tip becomes blunt. In front of the plastic region, phase transformation from the original bcc structure to fcc structure has been formed. This stress-induced phase transformation has been observed by several authors[27–31] at the crack tip in bcc iron. With the grain boundary gliding, the opening of the crack tip becomes wider and wider. At the time of 40 ps (see Fig. 2(c)), there are considerable atomic planes that glide out of the two boundaries of the model and formed two steps at the two boundaries of the model. As the result of the crack blunting, propagation of the original crack along the direction perpendicular to the grain boundary almost stops and the crack propagates mainly by a grain boundary gliding manner.

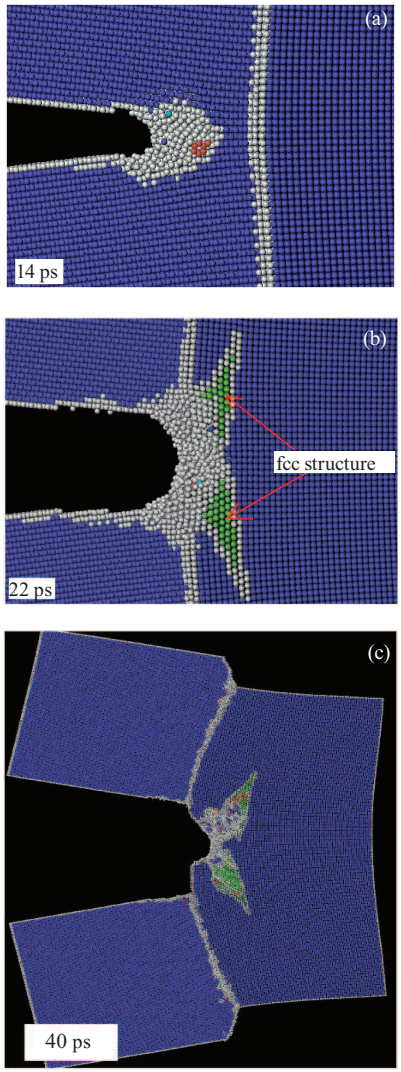


Fig. 2. (color online) Crack's atomistic configuration of model A at (a) 14, (b) 22, and (c) 40 ps.

3.1.2. Model B

Figure 3 presents the atomistic process of the crack propagation through the {001}/{110} grain boundary from the {110} part to the {001} part (the parts on both sides of the grain boundary are specified by the crystal orientations that are parallel to the x direction). The initial crack type is $\{1\bar{1}0\}\langle 001\rangle$ (specified by the crack plane and the crack front). From Fig. 3(b), we can find that before the crack reaches the grain boundary, the crack propagates forward in a cleavage manner. At the two sides of the crack tip, there are two regions shaped like the cusp of the moon, in which phase transformation from the original bcc structure to fcc structure can be found; the stress-induced phase transformation is recoverable to bcc structure when the crack tip moves away from this region. When the plastic region reaches the grain boundary, the grain boundary begins to glide, and hence the crack tip becomes blunt (see Fig. 3(b)). With the gliding of the grain boundary, the opening of the crack tip becomes wider and wider (the same as model A). In the front of the crack tip a

plastic region is formed because of the stress concentration in this region. Subsequently, the stress in the plastic region is relaxed by emitting some dislocations. As long as the gliding of the grain boundary begins, the crack stops propagating along the direction perpendicular to the grain boundary and turns its way along the grain boundary. Finally, the crack propagates in a grain boundary gliding manner (see Fig. 3(c)).

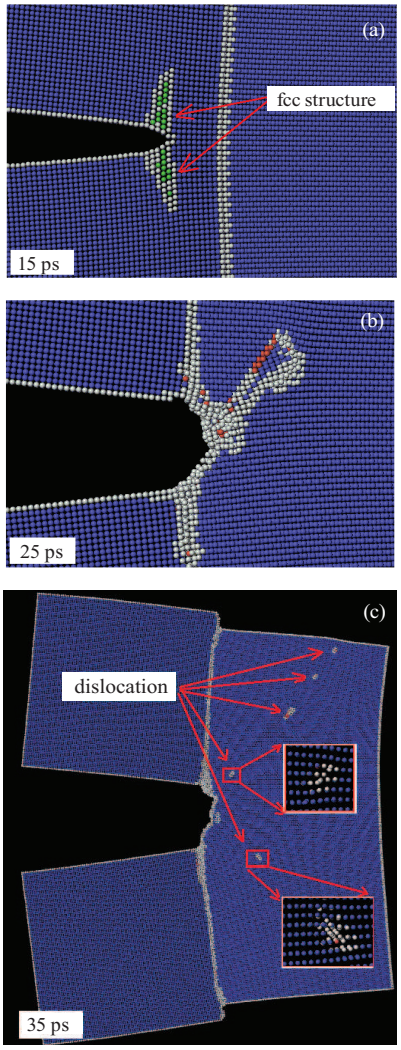


Fig. 3. (color online) Crack's atomistic configuration of model B at (a) 15, (b) 25, and (c) 35 ps.

Form the study of the above two models, we can find that the {001}/{110} type grain boundary can effectively arrest the crack that propagates along the direction perpendicular to the grain boundary by means of grain boundary gliding and increase the toughness of the model.

3.2. Effect of {110}/{111} grain boundary on the propagation of the crack

3.2.1. Model C

Figure 4 displays the details of the atomistic process of the crack propagation through the {110}/{111} grain boundary from the {110} part to the {111} part. The initial crack type is $\{1\bar{1}0\}\langle 001\rangle$, which is the same as the initial crack type of model B. From Fig. 4(a), we can find that before the crack reaches the grain boundary, the crack propagates forward in the same manner as the crack propagates in model B. When the crack tip reaches the grain boundary, the grain boundary begins to glide. As a result, the crack tip becomes blunt (see Fig. 4(b)). The blunting effect will relax the stress of the crack tip and stop the crack propagating forward. Subsequently, the direction of the crack turns from the direction perpendicular to the grain boundary to the direction along the grain boundary (see Fig. 4(c)), leading to the delamination crack.

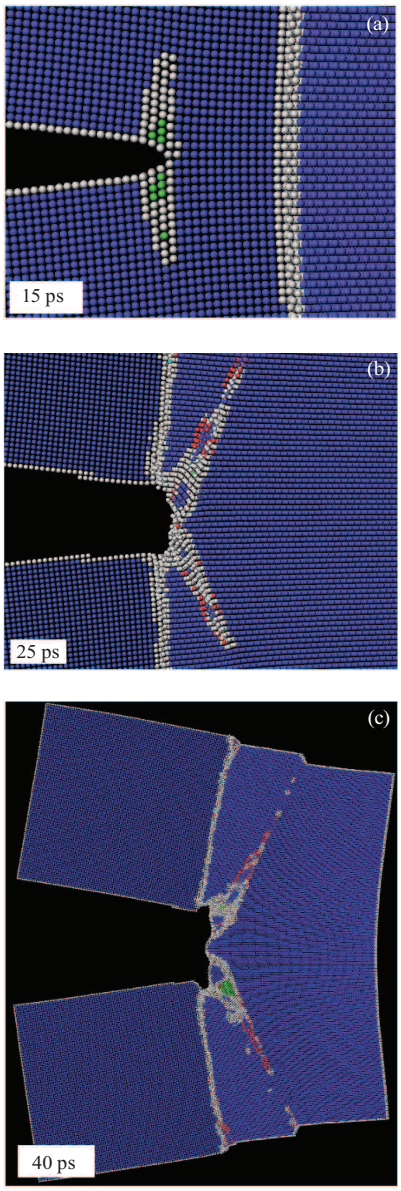


Fig. 4. (color online) Crack's atomistic configuration of model C at (a) 15, (b) 25, and (c) 40 ps.

3.2.2. Model D

Figure 5 presents the atomistic process of the crack propagation through the {110}/{111} grain boundary from the {111} part to the {110} part. The initial crack type is

$\{1\bar{1}0\}\langle 11\bar{2}\rangle$. Figure 5(a) gives the atomistic configuration of the crack at 10 ps. It can be clearly seen that before the crack reaches the grain boundary, the crack propagates forward in a cleavage manner, and is accompanied by two small plastic regions at the two sides of the crack tip. When the crack tip reaches the grain boundary, the crack tip becomes blunt by means of the gliding of the grain boundary (see Fig. 5(b)). With the concentration of the stress on the crack tip, the crack, which is accompanied by a plastic region and stress-induced phase transformation ahead of its tip, continues to propagate forward in the $\{110\}$ part. However, the blunt effect changes the propagation mode from complete cleavage to a little ductility, and improves the toughness of the iron.

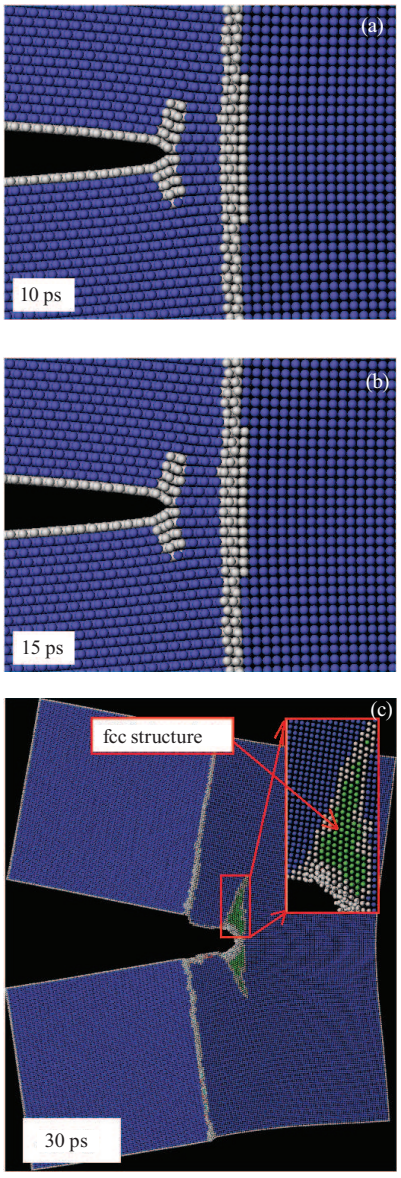


Fig. 5. (color online) Crack's atomistic configuration of model D at (a) 10, (b) 15, and (c) 30 ps.

From the studies of the models C and D, we can know that the $\{1\bar{1}0\}\langle 001\rangle$ and $\{1\bar{1}0\}\langle 11\bar{2}\rangle$ crack types propagate in a cleavage manner in single crystal at low temperature. However, the effect of the $\{001\}/\{110\}$ type of grain boundary gliding can remarkably change the fracture mode from brittleness to ductility, and improve the low-temperature toughness of the iron.

3.3. Effect of $\{001\}/\{111\}$ grain boundary on the propagation of the crack

3.3.1. Model E

Figure 6 presents the details of the atomistic process of the crack propagation through the $\{001\}/\{111\}$ grain boundary from the $\{111\}$ part to the $\{001\}$ part. The initial crack type is $\{1\bar{1}0\}\langle 11\bar{2}\rangle$. Figure 6(a) is the atomistic configuration

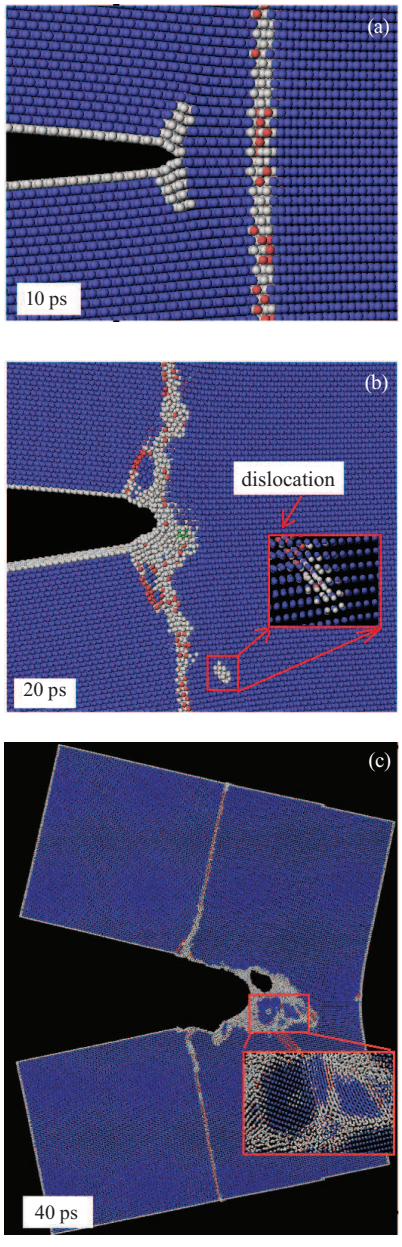


Fig. 6. (color online) Crack's atomistic configuration of model E at (a) 10, (b) 20, and (c) 40 ps.

of the crack at 10 ps, from which we can find that before the crack reaches the vicinity of the grain boundary, the crack, which is accompanied by two small plastic regions at its tip, propagates forward in a cleavage manner, and leaves two mirror-like planes. When the crack tip arrives at the vicinity of the grain boundary (see Fig. 6(b)), two dislocations are emitted from both sides of the crack tip. Subsequently, the dislocation on the upper side of the crack tip is arrested by the grain boundary. On the contrary, the dislocation on the low side of the crack tip goes through the grain boundary and propagates in the $\{001\}$ part. Unlike the above four models (A, B, C, and D), the crack passes the grain boundary without the sliding of the grain boundary. Figure 6(c) gives the atomic configuration of the crack at 40 ps, from which it can be seen that ahead of the crack tip, there is a large plastic region where the nucleation of a nanovoid and recrystallization occur. With increasing load, the nanovoid becomes bigger and joins with the main crack. Subsequently, the crack propagates forward.

3.3.2. Model F

Figure 7 is the atomistic process of the crack propagation through the $\{001\}/\{111\}$ grain boundary from the $\{001\}$ part to the $\{111\}$ part. The initial crack type is $\{1\bar{1}0\}\langle 110\rangle$. From Fig. 7(a), it can be observed that a dislocation has been created from the crack tip and moves along the $\{112\}$ plane, is then arrested by the grain boundary, and the emission of the dislocation leads to the crack tip blunting. Before the crack reaches the grain boundary, a plastic region exists in front of the crack tip, and the atom in this region is disordered rather than keeping bcc structure (similar to model A). When the crack tip arrives at the grain boundary, the stress in the plastic region accumulates high enough to generate two long strips of twins in the $\{111\}$ part, and this makes the crack open wider. After the crack tip passes the grain boundary, the plastic region ahead of the crack tip becomes larger and the crack propagates forward into it. From Fig. 7(c), we can clearly see that the sliding of the grain boundary does not appear in the model during the simulation process.

From the studies of the models E and F, we can find that the $\{001\}/\{111\}$ grain boundary does not slide when the crack tip arrives at it, so this type of grain boundary has little role in improving the low temperature toughness of the iron.

3.4. Mechanism of sliding of grain boundary

3.5. Dislocation mechanism of the grain boundary sliding

From the above simulations, it can be found that the sliding of the $\{001\}/\{110\}$ and $\{110\}/\{111\}$ type grain boundary can blunt the crack and improve the impact toughness. Grain boundary sliding means a shearing of neighboring grains with respect to each other, which is localized in their GBs. From a microscopic viewpoint, there are two mechanisms of grain boundary sliding: one is the movement of GB dislocations;[32,33] the other is local shear events which represent either individual atomic jumps or local transformations of small groups of atoms in the grain boundary phase.[34–37] Therefore, we will solve the question of which mechanism controls the grain boundary sliding of the present work.

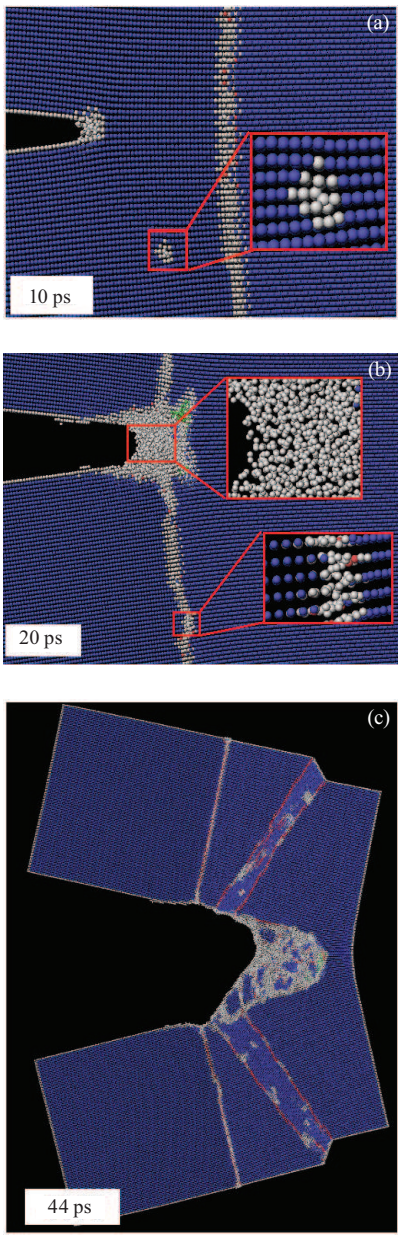


Fig. 7. (color online) Crack's atomistic configuration of model F at (a) 10, (b) 20, and (c) 44 ps.

Figure 8 displays the upper part of the crack model B at 20 ps, from which we can find that the crack tip is blunted by the sliding of the $\{001\}/\{110\}$ grain boundary. In order to study the mechanism of the grain boundary sliding, two local parts of the grain boundary are enlarged. From the enlarged parts, we can see clearly that there is one edge dislocation in each enlarged part, which can prove that the sliding of the $\{001\}/\{110\}$ grain boundary is realized by means of the motion of dislocation along the grain boundary. We have also

studied the sliding of the grain boundary in the above cracked model A, model C, and model D, and found that all the grain boundary sliding in these models is realized by means of the motion of dislocation along the grain boundary. Thus, we can conclude that the mechanism of the grain boundary sliding in this work is the motion of dislocation along the grain boundary.

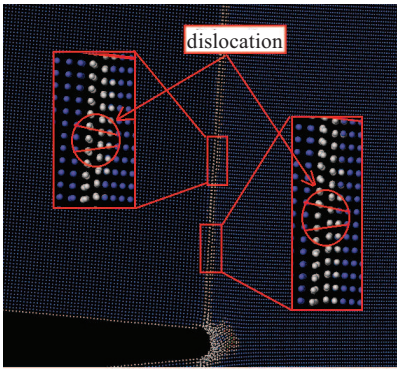


Fig. 8. (color online) The atomistic configuration of model B at 20 ps. The two enlarged parts show the dislocations, which originate from the crack tip and slide along the {001}/{110} grain boundary.

3.6. Energy analysis of the grain boundary sliding

In order to study the underlying cause of the grain boundary sliding we have calculated the generalized stacking fault (GSF) energy of the grain boundary, which is a total energy variation ($\Phi(R)$) under the rigid shift of one part of the crystal relative to another at a fault vector R along the $[1\bar{1}0]$ direction. To be consistent with the above cracked models, we construct three kinds of grain boundary model with the same orientations as the above cracked models A, C, and E, respectively. Each model is divided into two parts by grain boundary; the part on one side of the grain boundary is fixed and the part on the other side of the grain boundary is gradually displaced along the $[1\bar{1}0]$ direction. During this rigid sliding, the GSF energy can be calculated by

$$\Phi(R) = (E_{\rm pot}(R) - E_{\rm pot}(0))/S, \qquad (2)$$

where R is the relative shear displacement between the lower fixed part and the upper moving part, S is the total area of the $(11\bar{1})$ plane, $E_{\rm pot}(R)$, and $E_{\rm pot}(0)$ are the potential energies of the system at the relative shear displacement R and 0, respectively.

Figure 9 shows the GSF energy as a function of the dimensionless shear displacement during the rigid sliding of the lower (fixed) and upper (moving) parts of the crystal. The energies located at $0.5b$ ($b = \sqrt{2}a_0$, with a_0 being the lattice constant of Fe) are the unstable stacking energies, which represent the energy barrier for grain boundary slipping. It can be found that the unstable stacking energies of the {001}/{110}, {110}/{111}, and {001}/{111} grain boundaries are 3.93, 3.74, and 19.42J/m^2, respectively. That is to say, the unstable stacking energies of the {001}/{110} and {110}/{111} grain boundaries are almost equal to a fifth of the unstable stacking energy of the {001}/{111} grain boundary. Therefore, the {001}/{110} and {110}/{111} grain boundaries are easier to slide than the {110}/{111} grain boundary under the shear stress. This is the reason why the {001}/{110} and {110}/{111} grain boundaries can slide under the shear stress of the crack tip and the {110}/{111} grain boundary cannot.

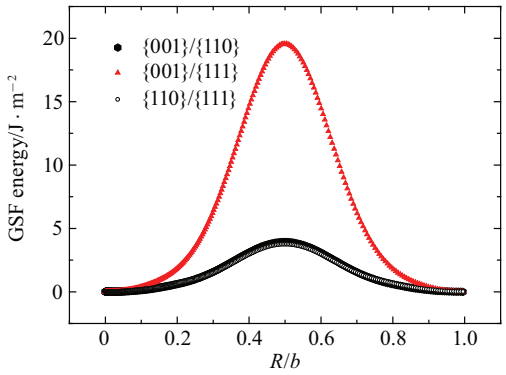


Fig. 9. (color online) Generalized stacking fault energy as a function of the dimensionless shear displacement during the rigid sliding. The R is the relative shear displacement between the lower fixed part and the upper moved part.

Based on the above simulations and energy analysis, the sliding of {001}/{110} and {110}/{111} grain boundaries plays an important role in arresting the propagation of the crack (along the SD) which is perpendicular to the grain boundary (along the RD), and increases ductility of the material. The similar mechanism of improving ductility by sliding of the grain boundary was also addressed by Farkas in the study of fracture resistance of nanocrystalline Ni.[38] When the propagation of the crack along the SD is arrested by the grain boundary sliding, the crack will propagate in a grain boundary sliding manner (model A and model B) or by delamination of the grain boundary manner (model C), and this will dramatically enhance the low-temperature impact toughness of the steel. Furthermore, the ultrafine grain structure bcc steel bar was analysed by EBSD, and it was found that the intensities of the SD//$\langle 101\rangle$ crystal orientations are larger than those of the SD//$\langle 001\rangle$ crystal orientations and those of the SD//$\langle 111\rangle$ crystal orientations.[14] From the analysis of the EBSD, we can deduce that the quantity of the {001}/{110} type and {110}/{111} type grain boundary is larger than that of the {001}/{111} grain boundary. This can increase the probability of the grain boundary sliding and contribute to impact toughness. Moreover, the ultrafine grain structure bcc steel bar has an ultrafine elongated grain structure, and the average grain size in the SD direction is 260 nm.[13] This ultrafine grain structure along the SD and elongated along the RD can

increase the quantity of the grain boundary along the SD and elongate the free gliding distance of the grain boundary (along the RD). Therefore, it is another key factor to improve the impact toughness of the ultrafine grain structure bcc steel bar.

4. Conclusions

In this paper, molecular dynamics simulations are used to investigate the mechanisms of low-temperature impact toughness of the ultrafine grain structure steel. Firstly, based on the analysis of EBSD, six cracked models are constructed to study the effect of the grain boundary on the impact toughness of the ultrafine grain structure steel. The simulations suggest that the sliding of the {001}/{110} type and {110}/{111} type grain boundaries can arrest the cracks which propagate along the SD direction, sometimes leading to the crack propagating along the grain boundary, forming a delamination crack at the grain boundary, and improving the impact toughness. However, the {001}/{111} type grain boundary cannot slip along the grain boundary and has no contribution to the impact toughness. Then, the mechanism of grain boundary sliding was studied, and it was found that the dislocations that nucleate at the crack tip and move along the grain boundary are the underlying cause of the grain boundary sliding. Finally, the sliding of the grain boundary was analyzed from the standpoint of the GSF energy and we found that the unstable stacking energies of the {001}/{110} and {110}/{111} grain boundaries are almost equal to a fifth of the unstable stacking energy of the {001}/{111} grain boundary. Therefore, the {001}/{110} and {110}/{111} grain boundaries are much easier to slide than the {110}/{111} grain boundary under the shear stress of the crack tip. Thus, we can draw a conclusion that the sliding of the {001}/{110} type and {110}/{111} type grain boundaries is one of the main factors to improve the low-temperature impact toughness of the ultrafine grain structure steel. The methods which can increase the quantity of the {001}/{110} type and {110}/{111} type grain boundaries and elongate the free gliding distance of these grain boundaries will improve the low-temperature impact toughness of the ultrafine grain structure steel.

References

[1] Morris Jr J W 2008 *Science* **320** 1022
[2] Pickering F B 1978 *Physical Metallurgy and the Design of Steels* (London: Applied Science Publishers) p. 16
[3] Gladman T and Pickering F B 1983 *The Effect of Grain Size on the Mechanical Properties of Ferrous Materials* (London: Applied Science Publishers) p. 14
[4] Takaki S, Kawasaki K and Kimura Y 2001 *J. Mater. Process. Technol.* **117** 359
[5] Morris Jr J W, Lee C S and Guo Z 2003 *ISIJ Int.* **43** 410
[6] Tsuji N, Okuno S, Koizumi Y and Minamino Y 2004 *Mater. Trans.* **45** 2272
[7] Song R, Ponge D and Raabe D 2005 *Acta Mater.* **53** 4881
[8] Stolyarov V V, Valiev R Z and Zhu Y T 2006 *Appl. Phys. Lett.* **88** 041905
[9] Karimpoor A A, Aust K T and Erb U 2007 *Scr. Mater.* **56** 201
[10] Shanmugam P and Pathak S D 1996 *Eng. Fract. Mech.* **53** 991
[11] Mintz B and Morrison W B 2007 *Mat. Sci. Tech.* **23** 1346
[12] Kimura Y, Inoue T, Yin F, Sitdikov O and Tsuzaki K 2007 *Scr. Mater.* **57** 465
[13] Kimura Y, Inoue T, Yin F and Tsuzaki K 2008 *Science* **320** 1057
[14] Inoue T, Yin F X, Kimura Y, Tsuzaki K and Shojiro Ochiai 2010 *Metallurgical and Materials Transactions A* **41** 341
[15] Kimura Y, Inoue T, Yin F X and Tsuzaki K 2010 *ISIJ Int.* **50** 152
[16] Zhang J M, Huang Y H, Xu K W and Ji V 2007 *Chin. Phys.* **16** 210
[17] Chen J, Chen D Q and Zhang J L 2007 *Chin. Phys.* **16** 2779
[18] Chen L Q, Wang C Y and Yu T 2008 *Chin. Phys. B* **17** 662
[19] Li L, Shao J L, Li Y F, Duan S Q and Liang J Q 2012 *Chin. Phys.* B **21** 026402
[20] Plimpton S 1995 *J. Comput. Phys.* **117** 1
[21] Plimpton S 2007 *Large-Scale Atomic/Molecular Massively Parallel Simulator* (Sandia National Laboratories)
[22] Mendelev M I, Han S, Srolovitz D J, Ackland G J, Sun D Y and Asta M 2003 *Philos. Mag.* **83** 3977
[23] Malerba L, Marinica M C, Anento N, Björkas C, Nguyen H, Domain C, Djurabekova F, Olsson P, Nordlund K, Serra A, Terentyev D, Willaime F and Becquart C S 2010 *J. Nucl. Mater.* **406** 19
[24] Sih G C and Liebowitz H 1968 *Mathematical Theories of Brittle Facture* (New York: Academic Press)
[25] Cleveland C L, Luedtke W D and Landman U 1999 *Phys. Rev.* B **60** 5065
[26] Alexander S 2010 *Modelling Simul. Mater. Sci. Eng.* **18** 015012
[27] Bancroft D, Peterson E and Minshall S 1956 *J. Appl. Phys.* **27** 291
[28] Zhang J and Guyot F 1999 *Phys. Chem. Miner.* **26** 419
[29] Fujiwara H, Inomoto H, Sanada R and Ameyama K 2001 *Scr. Mater.* **44** 2039
[30] Nishimura K and Miyazaki N 2001 *Comput. Model. Eng. Sci.* **2** 143
[31] Kadau K, Germann T C, Lohmdahl P S and Holian B L 2002 *Science* **296** 1681
[32] Sutton A P and Balluffi R W 1996 *Interfaces in Crystalline Materials* (Oxford: Oxford Science Publications)
[33] Gutkin M Yu and Ovidko I A 2004 *Plastic Deformation in Nanocrystalline Materials* (Berlin: Springer)
[34] Conrad H and Narayan J 2000 *Scr. Mater.* **42** 1025
[35] van Swygenhoven H and Derlet P A 2001 *Phys. Rev.* B **64** 224105
[36] Padmanabhan K A and Gleiter H 2004 *Mater. Sci. Eng.* A **381** 28
[37] Demkowicz M J, Argon A S, Farkas D and Frary M 2007 *Philos. Mag.* **87** 4253
[38] Farkas D 2007 *Metallurgical Mater. Trans.* A **38** 2168